Effect of material, geometry, surface treatment and environment on the shear strength of single lap joints

Lucas F M da Silva[1,*], R J C Carbas[1], G W Critchlow[2], M A V Figueiredo[1] and K Brown[3]

[1]**Departamento de Engenharia Mecânica e Gestão Industrial, Faculdade de Engenharia, Universidade do Porto**

Rua Dr. Roberto Frias, 4200-465 Porto, Portugal

[2]**Institute of Surface Science & Technology, Loughborough University**

Loughborough, Leicestershire LE11 3TU, UK

[3]**Chemetall PLC, Denbigh Road, Bletchley, Milton Keynes MK1 1PB, UK**

Abstract

The single lap joint is the most studied type of adhesive joint in the literature. However, the joint strength prediction of such joints is still a controversial issue as it involves a lot of factors that are difficult to quantify such as the overlap length, the yielding of the adherend, the plasticity of the adhesive and the bondline thickness. The most complicated case is that where the adhesive is brittle and the overlap long. In any case, there is still a problem that is even more difficult to take into account which is the durability. There is a lack of experimental data and design criteria when the joint is subjected to high, low or variable temperature and/or humidity. The objective of this work is to carry out and quantify the various variables affecting the strength of single lap joints in long term, especially the effect of the surface preparation. The Taguchi method is used to decrease the number of experimental tests. The effect of material, geometry, surface treatment and environment is studied and it is shown that the main effect is that of the overlap length.

---

[*] Corresponding author. Tel: +351225081706. Fax: +351225081445. Email: lucas@fe.up.pt

In order to quantify the influence of the adhesive (toughness and thickness), the adherend (yield strength and thickness), the overlap, the test speed, the surface preparation and durability on the lap shear strength, the experimental design technique of Taguchi was used in the present study. An experimental matrix of eighteen tests was designed and each test was repeated three times. The influence of the eight previously-mentioned variables could be assessed using the statistical software Statview®. In this paper a simple predictive equation is proposed for the design of single lap joints.

Keywords

Adhesive; Adherend; Adhesive thickness; Overlap; Surface treatment; Durability; Lap shear strength; Statistical analysis.

1 Introduction

The single lap joint (SLJ) is very common in practice and simple design rules should be available for design purposes. Hart-Smith **[1]** proposed a chart where the joint strength is given as a function of adhesive ductility and overlap. The adherend is supposed to remain in the elastic range. This is not realistic since the substrates will yield in many cases (e.g. aluminium or low strength steel). The ASTM 1002 standard proposes a very simple design rule to guarantee that the adherends do not yield. Adams *et al.* **[2]** developed a simple methodology to predict the joint strength. If the adhesive is very ductile, typically with more than 20% shear strain to failure, and the adherends are elastic, the joint strength is given by the load corresponding to the total plastic deformation. If the adherends yield, the joint strength is governed by the

adherends yielding independently of the type of adhesive. For the case of a rather brittle adhesive and elastic adherends, the methodology does not work and Adams *et al.* **[2]** proposed the finite element method. The above simple design rules are very useful and can give a good prediction for many cases. There are, however, a number of parameters that are not considered in previous studies such as the adhesive thickness, the type of surface treatment and the durability.

The adhesive thickness has an important effect on the joint strength. Experience shows that the lap joint strength increases as the bondline gets thinner **[3-4]**. Several arguments have been proposed in the literature to explain the influence of the bondline thickness. Adams and Peppiatt **[3]** attribute the joint strength decrease with adhesive thickness to the fact that thicker bondlines contain more defects such as voids and microcracks. Crocombe **[5]** explains that as the adhesive gets thicker, the plastic spreading of the adhesive along the overlap occurs more rapidly. Interface stresses were shown to be higher for thicker bondlines by Gleich *et al.* **[6]** and da Silva *et al.* **[4].** More recently, Grant *et al.* **[7]** explained the influence of the adhesive thickness with the bending moment. For a lap joint under tension, the longitudinal stress from the direct load and the bending moment at the edge of the overlap region create plastic strains when the steel becomes plastic and these cause failure in the adhesive. The lap joint under tension is very sensitive to adhesive thickness. There is a longitudinal stress from the direct load together with an additional bending stress due to the load offset which is superimposed on the tension stress. To reach the same stress level, as the bending moment increases, the smaller the stress due to direct load has to be. As the bondline thickness increases, there is an increase in the bending stress since the bending moment has increased. Consequently the strength of the joint is reduced.

The adherend thickness is also important for two reasons **[8]**. For low strength adherends, an increase in thickness is beneficial because the adherend becomes stronger and less likely to deform plastically. On the other hand, for high strength adherends, a higher thickness can decrease the joint strength due to an increase of the bending moment.

The presence, or otherwise, of a surface treatment is another parameter that can significantly affect the joint strength. Most results in the literature are for mechanical treatments such as shot-blasting **[8-10]**. In the case of steel, which is the type of substrate studied here, chemical conversion coatings offer several advantages such as high treatment rates, good uniformity, and, particularly, the increased durability in adverse environments where the treatment confers a degree of corrosion protection preventing joint failure through the resultant friable hydrated metal oxide **[9-10]**.

The objective of the present study was to quantify the influence of the adhesive, the adherend, the adherend and adhesive thicknesses, the overlap, the surface treatment and the durability on the lap shear strength by using the Taguchi method **[11]** and to propose a simple predictive equation that work for any type of situation. A similar study was carried out by the authors in **[12]** and it was found that the surface treatment had little effect. However, the effect of the durability was not investigated. The main purpose of the present study is to extend the previous study and assess if the previous results are valid when durability is involved. The test speed was also investigated to assess any viscoleastic behaviour.

2 Experimental programme

2.1 Materials

Three adhesives were selected: a very ductile polyurethane adhesive (Sikaflex-255 FC); a very brittle two-component epoxy adhesive (Araldite® AV138/HV998 from Huntsman), and an intermediate two-component epoxy adhesive (Araldite® 2015 from Huntsman). The adhesives were tested in pure shear according to the thick adherend shear test (ISO 11003-2). The specimens were tested in an MTS servo-hydraulic machine 312.31 at a crosshead speed of 0.5 mm/min. Three specimens were tested for each adhesive. The shear mechanical properties of the adhesives used are shown in **Table 1**. The yield strength was calculated for a plastic deformation of 0.2% in the case of AV138/HV998. For the more ductile adhesives the yield strength was considered to be equal to the shear strength. To quantify the type of adhesive, the toughness was used by measuring the critical strain energy release rate in mode I (G_{Ic}) with the double cantilever beam specimen (ASTM D3433-99). The specimens were tensile tested in an MTS servo-hydraulic machine 312.31 at a crosshead speed of 1 mm/min. Three specimens were tested for each adhesive. The results are presented in **Table 2**.

The adherends selected were a low strength steel (DIN St33) with σ_{ys} = 184 MPa and a high strength steel (DIN C65 heat treated) with σ_{ys} = 1260 MPa.

2.2 Joint geometry

The single lap joints (SLJ) had an overlap of 12.5, 25 or 50 mm and a width of 25 mm; see geometry in **Figure 1**. The adherend thickness was 1, 2 or 3 mm. The SLJs were manufactured individually in a mould and the adhesive thickness was controlled by packing shims. Three values of adhesive thickness were used: 0.5, 1 and 2 mm.

2.3 Surface treatment

2.3.1 Mechanical treatment (P)

The bonding area was initially degreased with acetone, abraded with a #180 SiC sandpaper and again cleaned with acetone before the application of the adhesive.

2.3.2 Chemical conversion coating (A1)

In all cases, process chemicals used (Gardoclean S5174, Gardobond 901, Gardolene D 6800, Gardolene V6513 and Gardobond R2604) were from Chemetall Ltd (Milton Keynes, UK). Mild steel coupons were first spray cleaned with degreaser Gardoclean S5174, a proprietary process, at a concentration of 30 $g \cdot l^{-1}$ at 50ºC for 2 minutes. This was followed by a cold water rinse. Coupons were then sprayed at 70ºC, for 30 seconds with Gardobond 901 to produce an amorphous phosphate coating. A nominal coating weight of approximately 0.4 $g \cdot m^{-2}$ was produced. A further cold water rinse was carried out. A second treatment with Gardolene D 6800 was then carried out. This is a liquid, acidic, chromium-free, reactive final seal for phosphate-based conversion coatings, applied by immersion. Gardolene D6800 was applied from solution at a concentration of 1.6 $g \cdot l^{-1}$ in demineralised water at pH 4.2-4.8 for 30 seconds. Gardolene D 6800 improves the corrosion resistance as well as adhesion of conversion coated metal surfaces that are subsequently coated with conventional organic coatings. Coupons were then air blown and oven dried.

The hard steel was treated as above but was pickled in 16% HCl for 15 minutes followed by rubbing with a very fine grade wire wool to deoxidise and to desmut prior to Gardoclean S5174 application.

2.3.3 Chemical conversion coating (A2)

The cleaning and pickling stages detailed above for treatment A1 were used. Following these, conditioning was carried out in Gardolene V6513, a titanium phosphate refiner, applied at a concentration of 0.4 $g \cdot l^{-1}$ in demineralised water for 30 seconds. Then this immersion was carried in Gardobond R2604, a trication zinc phosphate, at 53ºC for 3 minutes. This produces a film of nominal coating weight 2.9 $g \cdot m^{-2}$. Panels were then cold water rinsed, air dried and oven dried, as in treatment A1.

2.4 Ageing conditions

The joints were subjected to 50ºC and a relative humidity (RH) of 80% for 0, 1 and 4 weeks. A Weiss Technik chamber SB 500 was used.

2.5 Test conditions

The specimens were tested in an MTS servo-hydraulic machine 312.31 with a load cell of 250 kN. The test speed was 1, 10 or 100 mm/min and 25% of the maximum load cell capacity was used for test recording. Three specimens were tested for each case. Tab ends were used to improve alignment, as shown in **Figure 1**.

2.6 Taguchi matrix

The Taguchi method was used to design the experiments. The Taguchi array contains eight factors, or variables, corresponding to the adherend yield strength, the adherend thickness, the adhesive thickness, the overlap, the adhesive toughness, the test speed, the surface treatment and the durability. If all the possible test combinations were to

be tested, the number of tests would be 4374 which is impractical in terms of time and cost. The use of pre-defined orthogonal arrays on which the Taguchi method is based reduces the number of tests and permits to quantify the interactions between the variables considered **[14]**.

The L_{18} (2^1 x 3^7) array was selected **[15]** (see **Table 3**). It contains 18 rows corresponding to the number of tests, one column with two levels (adherend yield strength) and 7 columns with 3 levels. The first column was assigned to the adherend yield strength (σ_{ys}), the second to the overlap (l), the third to the adherend thickness (t_s), the fourth to the adhesive thickness (t_a), the fifth to the adhesive toughness (G_{Ic}), the sixth to the surface treatment (S_T), the seventh to the durability parameter (A) and the eighth to the test speed (V). The response studied was the failure load in the lap shear tests. Interactions between three-level columns are distributed more or less uniformly to all other three-level columns, which permits investigation of main effects. Thus, it is a highly recommended array for reducing the number of experiments **[14]**. It is, however, possible to assess the interaction between the first (adherend yield strength) and second column (overlap) which was done here.

The influence of each variable and the interaction was assessed by the average response and the analysis of variance (ANOVA). The statistical software Statview® (SAS Institute, Inc., Cary, NC, USA) was used.

2.7 Surface analysis

Surface analysis was carried out to identify the changes introduced to the steel substrate by the different pretreatments. Scanning electron microscopy (SEM) and white light interferometry (WLI) were used to study the surface topography whilst Auger electron spectroscopy (AES) was used to determine surface chemistry.

2.7.1 White light interferometry (WLI)

WLI was carried out using a Zygo NearView 5000 interferometer. Several areas on each sample were scanned using a raster width of 520 by 690 μm.

2.7.2 Scanning electron microscopy (SEM)

SEM was conducted using a Leo 1530 VP instrument using a primary beam energy of 10×10^{3} eV and a current of approximately 200×10^{-12} A.

2.7.3 Auger electron spectroscopy (AES)

A Joel JAMP 7100 AES spectrometer was used. The primary beam energy was 10×10^{3} eV with a current of 0.7×10^{-6} A. Compositions were determined using experimentally derived relative sensitivity factors based upon ZrO_2 and P_2O_5 reference materials. In each case, two areas approximately 1 cm apart were analyzed with an analysis area of 100 μm across.

3 Results

3.1 Surface analysis

3.1.1 White light interferometry (WLI)

WLI images are given in **Figure 2** for mild steel and in **Figure 3** for high strength steel. A summary of roughness values from the aforementioned WLI data are given in **Table 4** in two different areas on each surface. The generally rougher, crystalline

surface texture introduced by A2 is confirmed by this analysis. The grooves from the sandpaper are clearly visible in **Figure 3a)** and **Figure 4a)**. For treatments A1 and A2, the mild steel surface is more irregular than that of the hard steel and rougher.

3.1.2 Scanning electron microscopy (SEM)

SEM images were obtained at both low and high magnifications on all surfaces. The low magnification images were used to determine the uniformity of treatments, in terms of area coverage, whilst the high-resolution images characterized the micro-rough features present. SEM images are presented in **Figures 4** to **6**.

Small sub-micrometer sized nodules were apparent, especially at high magnification, for the A1 process, see **Figure 4**. Such features might be responsible for the formation of an interphase with a subsequently applied adhesive. Many workers have identified the presence of an interphase as contributing towards good adhesion with metallic adherends. However, most A1 treated joints failed with an apparent interfacial failure.

The surface topography of the A2 treated substrates was highly crystalline, see **Figure 5**. The A2 treated joints gave an apparent interfacial failure, especially for adhesives AV 138 and 2015 and a mixed failure (interfacial and cohesive) for adhesive Sikaflex-255.

As indicated by SEM images in **Figure 6**, SEM indicated that the sandpaper treatment provided irregular scratches on a macro-rough scale. Good wettability was observed with triply-distilled water indicating that the adhesive would be expected to spread

well on such a relatively high-energy surface. Adherends prepared with sandpaper gave a cohesive failure for most of the cases.

3.1.3 Auger electron spectroscopy (AES)

In **Table 5**, data is given from one area only but there was very little area-to-area variation. The abraded material comprises carbon/calcium contaminated iron oxide with both steels. The treated surfaces have lower carbon levels and the presence of Zr, P and Zn from the conversion coating process. Note that these surfaces have relatively low carbon levels. The precise chemistry of the conversion coating solutions were not disclosed but it is possible that some of the carbon present might contain surface functionalisation suitable for reaction with subsequently applied adhesives or other organic coatings.

3.2 Lap shear strength

The experimental failure loads and the mode of failure of the SLJs are shown in **Table 3**. The failure load predicted using the simple design methodology proposed by Adams *et al.* **[2]** (see **Figure 7**) is also given in **Table 3**. The load corresponding to the total plastic deformation of the adhesive is given as:

$$F_{\mathrm{a}} = \tau_y \cdot w \cdot l \qquad \textbf{(2)}$$

where F_{a} is the failure load of the adhesive, τ_y is the shear yield strength of the adhesive, w is the joint width and l is the overlap length. The direct tensile stress (σ_t) acting in the adherend due to the applied load F is

$$\sigma_t = F \big/ \left(w \cdot t_s \right) \qquad \textbf{(3)}$$

where t_s is the adherend thickness. The stress at the inner adherend surface (σ_s) due to the bending moment M is

$$\sigma_s = 6M \Big/ \left(w \cdot t_s^{\,2} \right) \quad \textbf{(4)}$$

where $M = k \cdot F \cdot t_s / 2$, according to Goland and Reissner **[16]**. The variable k is the bending moment factor which decreases (from unity) as the lap rotates under load. The stress acting in the adherend is the sum of the direct stress and the bending stress. Thus, the maximum load which can be carried which just creates adherend yield (F_s) is:

$$F_s = \sigma_{ys} \cdot w \cdot t_s \Big/ \left(1 + 3k \right) \quad \textbf{(5)}$$

where σ_{ys} is the yield strength of the adherend. For low loads and short overlaps, k is approximately 1. Therefore, for such a case,

$$F_s = \sigma_{ys} \cdot w \cdot t_s / 4 \quad \textbf{(6)}$$

However, for joints which are long compared to the adherend thickness, such that l / $t_s \geq 20$, the value of k decreases and it is assumed here that it tends to zero. In this case, the whole cross section yields and:

$$F_s = \sigma_{ys} \cdot w \cdot t_s \quad \textbf{(7)}$$

The methodology proposed by Adams *et al.* **[2]** works reasonably well when there is yielding of the adherend. The adherend yielding appears clearly in the load-displacement curves presented in **Figure 8** for test nº 4 and 7 and is in accordance with **Equation 7**. **Figure 9** shows that the experimental points corresponding to mild steel compare reasonably well with the three curves corresponding to the predictions for t_s = 1, 2 and 3 mm using **Equations 6** and **7**. The predictions are slightly lower than the experiments because the initial yielding of the steel was used, ignoring the strain hardening of the steel. The points corresponding to tests nº 3 and 5 have not

been included because there was failure of the joint before plastic yielding of the adherends.

When the adherends remain in the elastic range, the methodology proposed by Adams *et al.* **[2]** may not give satisfactory results (see **Figure 10**). If the adhesive is very ductile (adhesives 2015 and Sikaflex-255), **Equation 2** gives a good prediction. But for brittle adhesives, like adhesive AV 138 and long overlaps, the methodology is not applicable. For this case, the Volkersen's model **[17]** was used and the failure occurs when the maximum shear stress at the ends of the overlap exceeds the shear strength of the adhesive. The following equation was used:

$$P = \tau_r \frac{2bl\sinh(\lambda l)}{\lambda l\left[1+\cosh(\lambda l)\right]} \qquad \textbf{(8)}$$

where

$$\lambda^2 = \frac{G}{t_a}\left(\frac{2}{Et_s}\right)$$

t_a is the adhesive thickness, G the adhesive shear modulus and E the adherend Young's modulus. This failure criterion works well when the adhesive is brittle, the steel is elastic and the failure is cohesive as in test nº 15. However, when the failure is adhesive (tests nº 3, 5, 10 and 13), the experimental joint strength is much lower than the prediction. The load/displacement curves presented in **Figure 11** are for tests nº 17 (AV138) and 18 (Sikaflex-255). In both cases the steel is elastic. The nonlinear behavior observed for test nº 18 is due to the adhesive deformation. Whereas the adhesive strength of the epoxy (AV138) is more than three times the strength of the polyurethane (Sikaflex-255), the strength of the adhesives in a joint is similar and the polyurethane adhesive has the advantage of being highly deformable.

Figure 12 presents typical failure surfaces of joints that failed cohesively in the middle of the adhesive **(Figure 12a)**, cohesively in the adhesive but close to the interface **(Figure 12b)** and adhesively **(Figure 12c)**.

3.3 Statistical analysis

3.3.1 Analysis of variance

The analysis of variance (ANOVA) (see **Table 6**) of the experimental results gives the relative importance of all the variables. The main factors influencing the failure load are the overlap (46%), the adhesive thickness (19%) and the adherend thickness (18%). The other factors are also significant in statistical terms but to a lesser degree being the sum of their contribution of approximately 17%. This result shows that the joint geometry is actually more important than the type of adhesive. Surprisingly, the surface treatment and the durability have very little influence. When compared with our previous study **[12]**, the influence of the overlap is this time much more important (20% in **[12]** against 40% in the present study). This can be explained by the fact that the adhesives used here are more ductile than those used in **[12]** and therefore make more use of the overlap. Another important difference with our previous results **[12]** is the effect of the adherend yield strength (19.7% in **[12]** against 3.8 in the present study). This might be due to the fact that in the present study a high number of cases for the high strength steel (cases 10, 13 and 16 in **Table 3**) had an adhesive failure giving a lower failure load than expected. This might have decreased the effect of the adherend yield strength.

The main effect of the adherend yield strength is shown in **Figure 13**. As expected, the failure load increases with the adherend yield strength. As the adherend plastic

deformation decreases, the adhesive can develop its full shear strength capacity and give a higher joint strength.

Figure 14 shows that the joint strength increases almost linearly with overlap. The overlap is the factor that has the biggest impact in the joint strength. This might be due to the fact that two ductile adhesives were used in the present study, which allow to use the whole overlap even for long overlaps.

The Taguchi array used here permits to evaluate the interaction between the adherend yield strength and the overlap, as shown in **Figure 15**. The graph failure load vs. overlap is nearly linear for the two types of adherend but the two lines are not parallel. The overlap effect increases as the adherend gets stronger. When the adherend is elastic, the adhesive can develop its full shear strength capacity and make use of the whole overlap. da Silva *et al.* **[18]** have shown this effect with more clarity for three different types of steels of increasing yield strength. They have also shown that there is interaction between adherend and adhesive and between adhesive and overlap but their percentage of contribution were low.

The main effect of the adherend thickness is presented in **Figure 16**. The increase is almost linear. This can be explained by the plasticity of the steel. As the adherend thickness increases, the resistant area of the steel increases and the adherend becomes stronger giving a chance to the adhesive to develop its full shear strength capacity. This, of course, is especially valid for the low strength steel because the high strength steel does not deform plastically for any thickness.

The influence of the adhesive thickness, presented in **Figure 17** confirms previous experimental results **[3, 4]**.

The effect of the adhesive toughness on the failure load is shown in **Figure 18**. The adhesive toughness increases the joint failure load up to 500 N/m and then there is a

decrease for the polyurethane adhesive which a fracture toughness of 2900 N/m. There seems therefore to be a peak corresponding to the best comprise between the adhesive toughness and the adhesive strength. The present Taguchi array is limited in terms of interactions assessment. However, da Silva *et al.* **[18]** have shown that for low strength steel, the failure load is independent of the adhesive; whereas for high strength steel, the failure load increases as the adhesive gets tougher.

Figure 19 gives the effect of the surface preparation. Surprisingly, the surface preparation has little effect on the joint strength. Even though the surface treatment results are not conclusive, **Figure 19** seems to indicate that treatments A1 and P are better than A2. This confirms previous results from reference **[10, 13]** with similar surface treatments.

The effect of the ageing is shown in **Figure 20**. The joint strength seems to be independent of the ageing conditions, at least for the conditions and times used here.

The test speed effect is also negligible (see **Figure 21**). This result is not surprising since all adhesives were used well below (case of epoxy adhesives 2015 and AV138) and well above (case of the polyurethane) their glass transition temperature where the viscoelastic effects are not substantial.

3.3.2 Linear regression

Two linear regressions were determined ($F_L^{\,1}$ and $F_L^{\,2}$). In the first linear regression, all the variables were used:

$$\begin{aligned} F_L &= M + (\overline{\sigma_{ysi}} - M) + (\overline{l_i} - M) + (\overline{t_{si}} - M) + \\ &+ (\overline{t_{ai}} - M) + (\overline{G_{Ici}} - M) + (\overline{S_{Ti}} - M) + (\overline{A_i} - M) + (\overline{V_i} - M) \end{aligned} \quad \textbf{(9)}$$

where F_L is the failure load prediction, M is the average failure load, $\overline{\sigma_{ysi}}$ is the adherend yield strength at level i, $\overline{t_{si}}$ is the adherend thickness at level i, $\overline{t_{ai}}$ is the adhesive thickness at level i, $\overline{l_i}$ is the overlap at level i, $\overline{G_{\mathrm{Ic}i}}$ is the adhesive toughness at level i, $\overline{S_{Ti}}$ is the surface treatment at level i, $\overline{A_i}$ is the durability al level i and $\overline{V_i}$ is the test speed at level i. The values of $\overline{\sigma_{ysi}}$, $\overline{l_i}$, $\overline{t_{si}}$, $\overline{t_{ai}}$, $\overline{G_{\mathrm{Ic}i}}$, $\overline{A_i}$ and $\overline{V_i}$ can be determined by the equation that best fits the data presented in **Figures 13**, **15, 16, 17, 19** and **20** respectively. The non quantitative variable surface treatment had to be treated with two dummy variables $M1$ and $M2$. Surface treatment P corresponds to $M1 = 0$ and $M2 = 1$, surface treatment A1 to $M1 = 1$ and $M2 = 0$ and surface treatment A2 to $M1 = 1$ and $M2 = 1$. The resulting equation is:

$$F_L{}^1 = 1,535 \times \sigma_{ys} + 166,442 \times l + 2156,871 \times t_s - 2148,964 \times t_a - \\ -0,490 \times G_{Ic} - 636,525 \times M1 - 813,590 \times M2 + 87,095 \times A + 5,884 \times V \quad \textbf{(10)}$$

where σ_{ys} is the adherend yield strength in MPa, t_s is the adherend thickness in mm, t_a is the adhesive thickness in mm, l is the overlap in mm, G_{Ic} is the critical strain energy release rate, $M1$ and $M2$ are the dummy variables defined above, A is the ageing in weeks and V is the test speed in mm/min. The square of coeffecient of correlation (R^2) was found to be 0.977.

The second linear regression was determined using the stepwise regression technique where in each step the most important variables (highest contribution) are tried in order to maximize the value of R^2. The regression was obtained in five steps and the following relation was obtained:

$$F_L{}^2 = 1,446 \times \sigma_{ys} + 162,171 \times l + 2050,100 \times t_s - 2255,735 \times t_a - 0,52390 \times G_{Ic} \quad \textbf{(11)}$$

A value of 0.973 was obtained for R^2, which is comparable to the first linear regression.

The two linear regressions defined above (**Equations 10** and **11**) were used to predict the failure load from tests available in the literature. **Table 7** shows that the predicted failure loads compare generally well with the experimental failure loads. This result shows that a statistical analysis can be an alternative method for the prediction of joint strength. The two equations give similar results and it is therefore advised to use **Equation 11** for its simplicity.

The results obtained in the present study were also used to reconfirm the validity of the linear regression obtained in **[12]** and to conclude about the most appropriate of the two linear regressions. The linear regression obtained in **[12]** is:

$$F_L = -6.625 + 0.005\sigma_{ys} + 5.225t_s - 7.359t_a + 0.161l + 0.519U_T \quad \textbf{(12)}$$

Note that in **[12]** the effect of the adhesive was taken as the area under the stress-strain curve (U_T). The U_T is just available for adhesives AV138/HV998 and 2015. **Table 8** shows that the failure prediction of **[12]** is valid and give similar results to those obtained with the present linear regression (see **Equation (11)** and **Table 3**), except for case 2. This is because **Equation (12)** was obtained for an adhesive thickness between 0.1 and 0.5 mm whereas case 2 has an adhesive thickness of 1 mm. This is an example where an extrapolation of the linear regression does not give satisfactory results. Therefore, due to its wider range of application, the linear regression of the present study (**Equation (11)**) is recommended. Moreover, the type of adhesive is better represented using G_{IC} than U_T.

4 Conclusions

SLJs made of carbon steel were studied. The effects of adherend yield strength, adherend thickness, adhesive thickness, overlap, adhesive toughness, surface

treatment, durability and test speed on the lap shear strength were investigated using the Taguchi method. The experimental results were statistically treated to give a failure load predictive equation. For the conditions tested here, the following conclusions can be drawn:

1. The lap shear strength increases with the overlap (45.5% contribution).
2. The lap shear strength decreases as the adhesive thickness increases (18.9% contribution).
3. The lap shear strength increases as the adherend thickness decreases (18.4% contribution).
4. The lap shear strength increases with the adherend yield strength (3.8% contribution).
5. The lap shear strength increases with the adhesive toughness from 346 N/m to 526 N/m and then decreases to 2902 N/m (5.5% contribution).
6. The effect of the surface treatment, durability and test speed are negligible.
7. The Taguchi method is a valid technique for lap shear strength prediction.

References

[1] Hart-Smith LJ. NASA Contract Report, NASA CR-112235, 1973.

[2] Adams RD, Comyn J, Wake WC. Structural adhesive joints in engineering, 2nd ed. London: Chapman & Hall, 1997.

[3] Adams RD, Peppiatt NA. J Strain Anal 1974; 9: 185.

[4] da Silva LFM, Rodrigues TNSS, Figueiredo MAV, de Moura MFSF, Chousal JAG. J Adhesion 2006; 82: 1091.

[5] Crocombe AD. Int J Adhes Adhes 1989; 9: 145.

[6] Gleich DM, van Tooren MJL, Beukers A. J Adhesion Sci Technol 2001; 15: 1091.

[7] Grant LDR, Adams RD, da Silva LFM. Int J Adhes Adhes 2008, doi:10.1016/j.ijadhadh.2008.09.001.

[8] Gledhill RA, Shaw SJ, Tod DA, Int J Adhes Adhes 1990; 10: 192.

[9] Critchlow GW, Webb PW, Tremlett CJ, Brown K. Int J Adhes Adhes 2000; 20: 113.

[10] Gan LM, Ong HWK, Tan TL. J Adhesion 1984; 16: 233.

[11] Taguchi G, Chowdhury S, Taguchi S. Robust engineering, New York: McGraw-Hill, 2000.

[12] da Silva LFM, Critchlow GW, Figueiredo MAV, J Adhesion Sci Technol 2008; 22 (13): 1477-1494.

[13] da Silva LFM, Adams RD, Gibbs M. Int J Adhes Adhes 2004; 24, 69.

[14] Ross PJ. Taguchi Techniques for quality engineering loss function, orthogonal experiments, parameter and tolerance design, New York: McGraw-Hill, 1991.

[15] Taguchi G, Konishi S. Orthogonal arrays and linear graphs, Dearborn, MI: ASI Press, 1987.

[16] Goland M, Reissner E. J Appl Mech 1944; 66: A17.

[17] Volkersen O. Luftfahrtforschung 1938; 15: 41.

[18] da Silva LFM, Ramos JE, Figueiredo MV, Strohaecker TR. J Adhesion and Interface 2006; 7, 1.

[19] Fowlkes WY, Creveling CM. Engineering methods for robust product design, Reading, MA: Addison-Wesley, 1995.

Table 1 Adhesive shear properties using the thick adherend shear test method ISO 11003-2 (three specimens tested for each temperature).

	Araldite® AV138M / HV998	Araldite® 2015	Sikaflex-255 FC
Shear modulus G (MPa)	1559 ± 11	487 ± 77	1.351 ± 0.04
Shear yield strength τ_{ya} (MPa)	25.0 ± 0.55	17.9 ± 1.8	8.26 ± 0.30
Shear strength τ_r (MPa)	30.2 ± 0.40	17.9 ± 1.8	8.26 ± 0.30
Shear failure strain γ_f (%)	5.50 ± 0.44	43.9 ± 3.4	330 ± 27

Table 2 Adhesive critical strain energy release rate in mode I (G_{Ic}) measured with the double cantilever beam ASTM D3433-99 (three specimens tested for each temperature).

	Araldite® AV138M / HV998	Araldite® 2015	Sikaflex-255 FC
Critical strain energy release rate in mode I G_{Ic} (N/m)	345.9 ± 47.8	525.7 ± 80.8	2901.1 ± 121.9

Table 3 Experimental plan based on Taguchi orthogonal array (L_{18}).

Test	σ_{ys}	l	t_s	t_a	G_{Ic}	S_T	A	V	F_L Experim.		F_L Predicted		Error
nº.	[MPa]	[mm]	[mm]	[mm]	[N/m]		[sem.]	[mm/min.]	[kN]	Mode	[kN]	Criterion	[%]
1	184	12.5	1	0.5	2902	P	0	1	2.36	DP/Coes	3.31	DP	40.3
2	184	12.5	2	1	526	A1	1	10	5.42	DP/Int	4.46	DP	17.7
3	184	12.5	3	2	346	A2	4	100	3.10	Ades			
4	184	25	1	0.5	526	A1	4	100	7.02	DP/Int	4.60	DP	34.5
5	184	25	2	1	346	A2	0	1	3.05	Ades			
6	184	25	3	2	2902	P	1	10	5.19	DP/Coes	6.90	DP	32.9
7	184	50	1	1	2902	A2	1	100	6.44	DP/Mist	4.60	DP	28.6
8	184	50	2	2	526	P	4	1	8.41	DP/Int	9.20	DP	9.4
9	184	50	3	0.5	346	A1	0	10	12.60	DP/Int	12.08	DP	4.1
10	1260	12.5	1	2	346	A1	1	1	1.81	Ades			
11	1260	12.5	2	0.5	2902	A2	4	10	3.84	Coes	2.58	CG	32.8
12	1260	12.5	3	1	526	P	0	100	6.97	Mist	5.60	CG	19.7
13	1260	25	1	1	346	P	4	10	5.24	Ades			
14	1260	25	2	2	2902	A1	0	100	4.48	Coes	5.16	CG	15.2
15	1260	25	3	0.5	526	A2	1	1	12.39	Coes	11.19	CG	9.7
16	1260	50	1	2	526	A2	0	10	6.12	Ades			
17	1260	50	2	0.5	346	P	1	100	13.67	Int	11.99	Volk	12.3
18	1260	50	3	1	2902	A1	4	1	11.40	Coes	10.33	CG	9.4

F_L - Failure load

Coes - Cohesive failure

DP - Plastic deformation of the steel

Int - Cohesive failure close to the interface

CG - Global yielding of the adhesive

Ades - Adhesive failure

Volk - Model of Volkersen

Mist - Mixed failure

Table 4 Summary of WLI topographical data – 520 μm x 690 μm scan.

	Treatment	Area	Area R_a (nm)	Area RMS (nm)	Max range R_z (nm)
Low strength steel	P	A	305	407	3301
		B	241	313	2910
	A2	A	331	448	3880
		B	288	418	5215
	A1	A	163	224	1639
		B	204	290	2299
High strength steel	P	A	203	270	2218
		B	199	262	1715
	A2	A	248	333	2980
		B	300	375	2320
	A1	A	153	222	2517
		B	223	282	1710

Table 5 AES data: surface composition atom%, excluding H and He.

Substrate	Treatment	C	Ca	O	Fe	Zr	P	Zn
Hard steel	P	51.4	3.3	28.2	17.1	0.0	0.0	0.0
	A1	17.0	1.8	51.6	6.4	9.3	10.1	3.7
	A2	21.6	0.0	41.9	3.1	5.6	13.8	14.1
Mild steel	P	36.6	4.8	36.7	22.0	0.0	0.0	0.0
	A1	14.2	2.2	51.4	11.5	10.4	7.7	2.6
	A2	26.2	0.0	41.2	0.0	8.1	5.6	18.9

Table 6 Analysis of variance (ANOVA) results.

Source	Sum of squares	Degrees of freedom	Mean square	F-value	P-value	% of contribution
σ_{ys}	35831282.2	1	35831280.0	320.6106	0.0001	3.8
l	426166569.1	2	213083300.0	1906.6236	0.0001	45.5
t_s	171951105.5	2	85975550.0	769.2908	0.0001	18.4
t_a	176921151.3	2	88460580.0	791.5263	0.0001	18.9
G_{Ic}	51724615.9	2	25862310.0	231.4104	0.0001	5.5
$_S T$	25921273.1	2	12960640.0	115.9690	0.0001	2.7
A	29737429.3	2	14868710.0	133.0420	0.0001	3.2
V	3208753.7	2	1604377.0	14.3556	0.0001	0.3
σ_{ys} * l	8145888.8	2	4072944.0	36.4438	0.0001	0.8
Residual (error)	6035013.5	54	111759.5			0.8
Total	935643082.2					100.0

Table 7 Experimental validation of the statistical failure load prediction.

Case	σ_{ys}	l	t_s	t_a	G_{Ic}	S_T	A	V	$F_L^{Experim.}$	F_L^{1}	Error 1	F_L^{2}	Error 2
	[MPa]	[mm]	[mm]	[mm]	[N/m]		[weeks]	[mm/min.]	[kN]	[kN]	[%]	[kN]	[%]
1	184	12.5	2	0.2	450	P	0	1	6.07	5.22	14.0	5.71	6.0
2	184	25	2	0.2	450	P	0	1	9.02	7.30	19.1	7.73	14.3
3	184	50	2	0.2	450	P	0	1	12.1	11.46	5.3	11.79	2.6
4	419	12.5	2	0.2	450	P	0	1	7.33	5.58	23.9	6.05	17.5
5	419	25	2	0.2	450	P	0	1	10.65	7.66	28.1	8.07	24.2
6	419	50	2	0.2	450	P	0	1	15.46	11.82	23.5	12.13	21.6
7	1078	12.5	2	0.2	450	P	0	1	6.37	6.59	3.5	7.00	9.9
8	1078	25	2	0.2	450	P	0	1	11.1	8.67	21.9	9.03	18.7
9	1078	50	2	0.2	450	P	0	1	16.88	12.83	24.0	13.08	22.5
10	184	25	1	0.2	346	A2	0	1	3.57	4.56	27.6	5.74	60.7
11	184	50	1	0.5	450	P	0	1	6.83	8.66	26.8	9.06	32.7
12	184	12.5	1.5	0.1	346	A2	0	1	3.58	3.77	5.3	4.96	38.6
13	184	25	1.5	0.2	450	P	0	1	8.55	6.22	27.2	6.71	21.5
14	184	50	2	0.2	346	A1	0	1	12.08	11.69	3.2	11.84	2.0
15	184	12.5	2	0.5	450	A2	0	1	3.47	3.94	13.5	5.03	45.0
16	1260	50	1	0.1	450	A2	0	1	6.56	10.53	60.6	11.52	75.6
17	1260	25	1	0.5	346	A1	0	1	4.84	6.38	31.8	6.62	36.7
18	1260	25	1.5	0.1	450	A1	0	1	16.05	8.26	48.5	8.49	47.1
19	1260	12.5	1.5	0.5	346	P	0	1	5.95	5.20	12.6	5.62	5.6
20	1260	50	2	0.1	346	P	0	1	15.37	13.38	13.0	13.62	11.4
21	1260	12.5	2	0.2	450	A1	0	1	11.91	7.05	40.8	7.26	39.0

Cases 1 to 9, see ref [19]
Cases 10 to 21, see ref [12]

Table 8 Validation of the statistical failure load prediction of **[12]** using the present experimental results.

Case (see **Table 3**)	σ_{ys}	t_s	t_a	l	U_T	S_T	$F_L^{Experim.}$	F_L (using **Eq. 12**)	Error
	[MPa]	[mm]	[mm]	[mm]	[MPa]		[kN]	[kN]	[%]
9	184	3	0.5	50	0.49	A1	12.6	10.43	17.18
17	1260	2	0.5	50	0.49	P	13.67	12.03	11.96
2	184	2	1	12.5	1	A1	5.42	-1.79	132.96
15	1260	3	0.5	25	1	A2	12.39	11.78	4.91

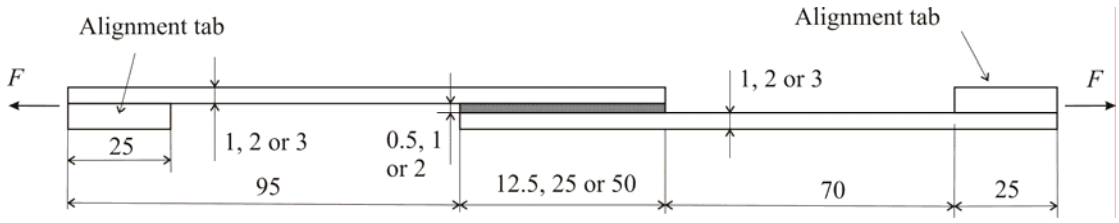

Figure 1 Single lap joints geometry (not to scale, dimensions in mm).

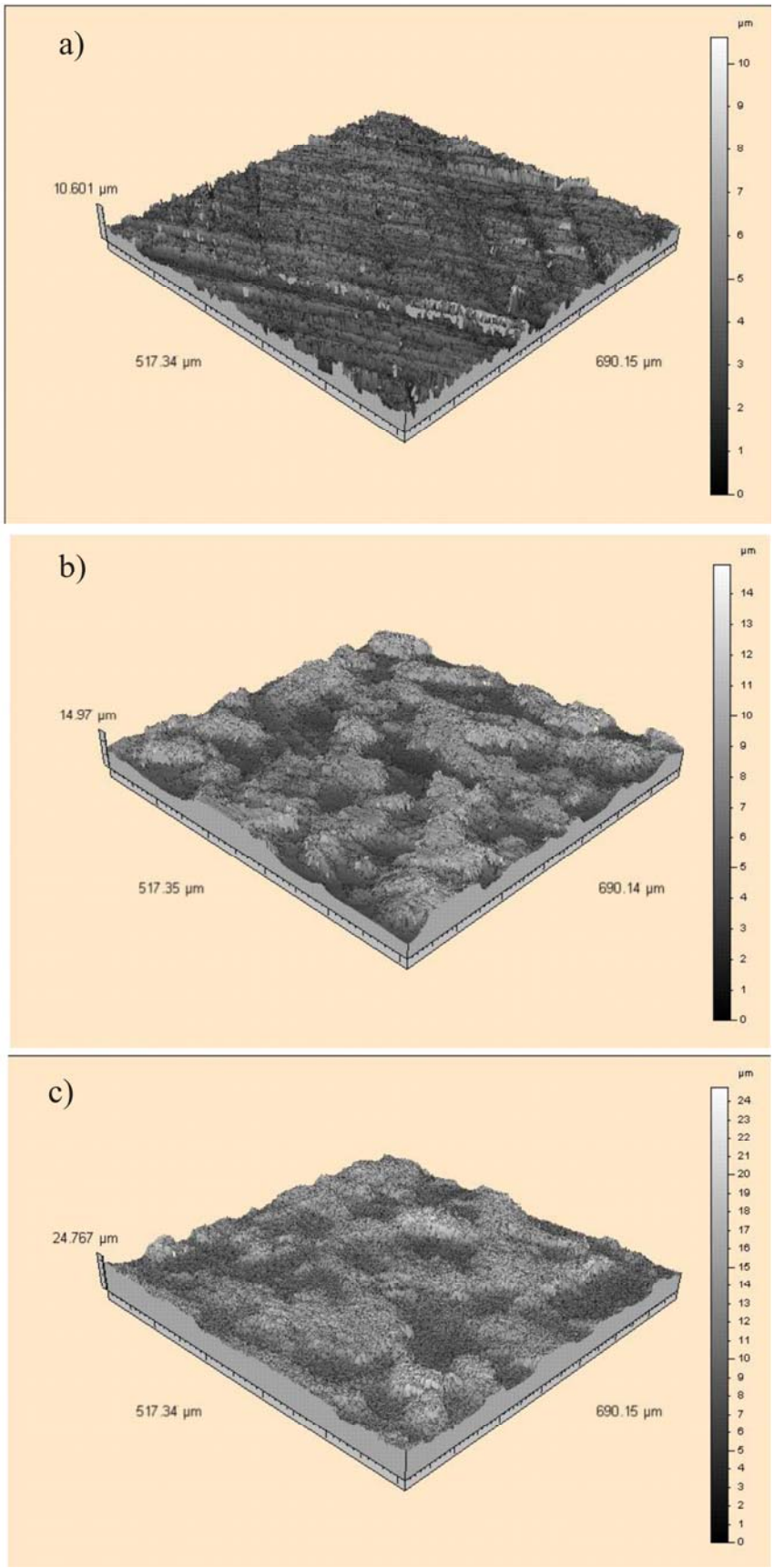

Figure 2 WLI images of low strength steel; a) from treatment P; b) from treatment A1; c) from treatment A2.

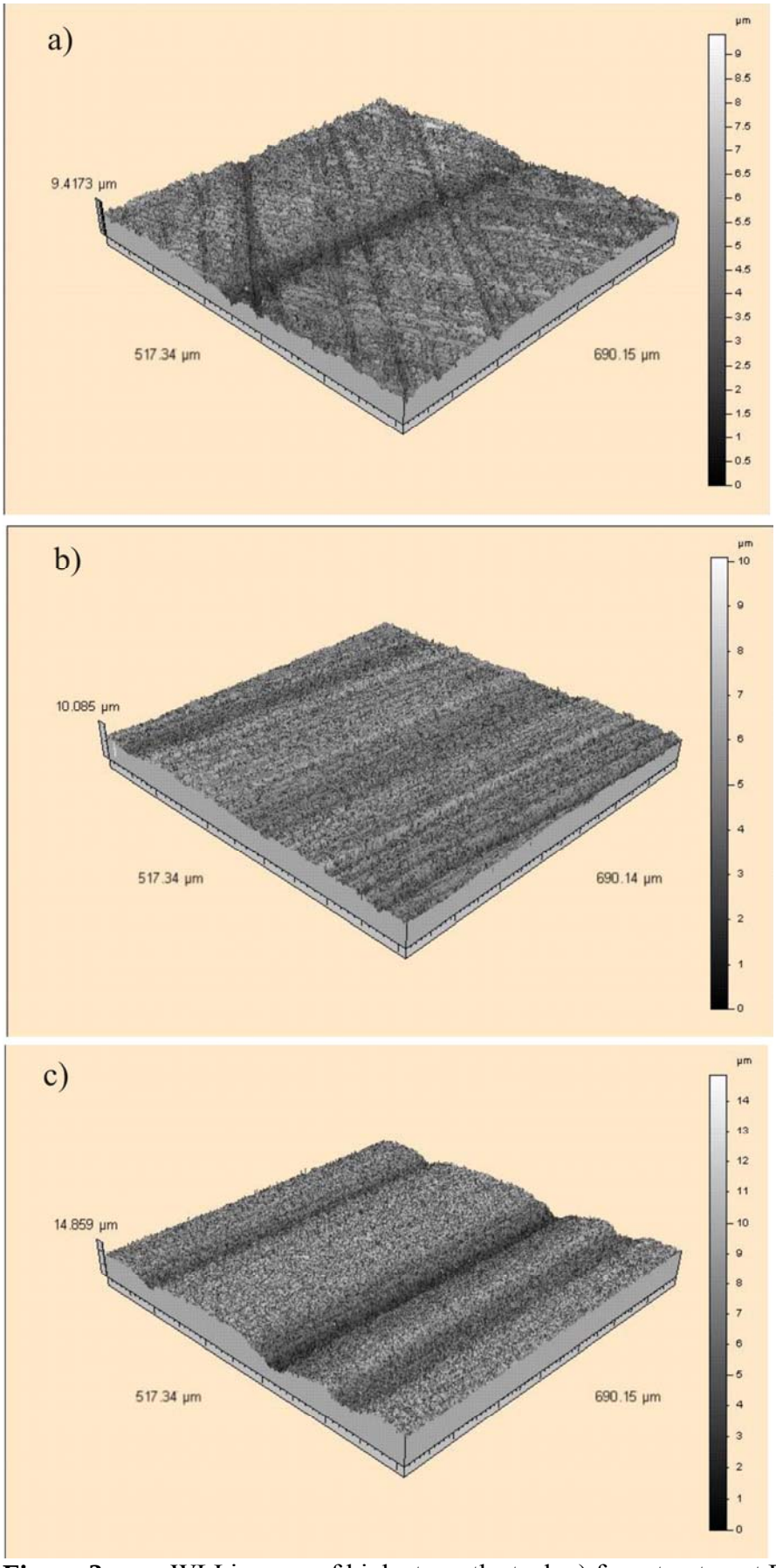

Figure 3 WLI images of high strength steel; a) from treatment P; b) from treatment A1; c) from treatment A2.

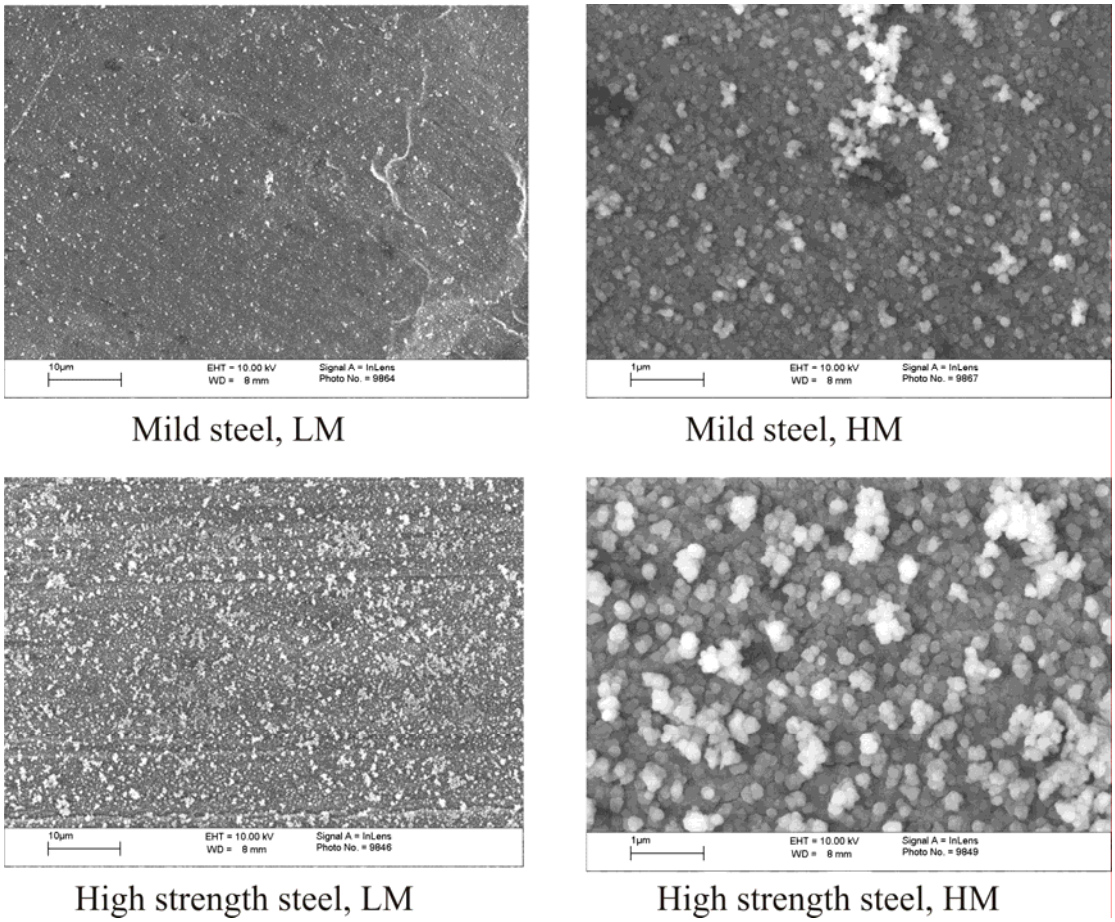

Figure 4 SEM images for A1 treatment of different steels (LM low magnification and HM high magnification).

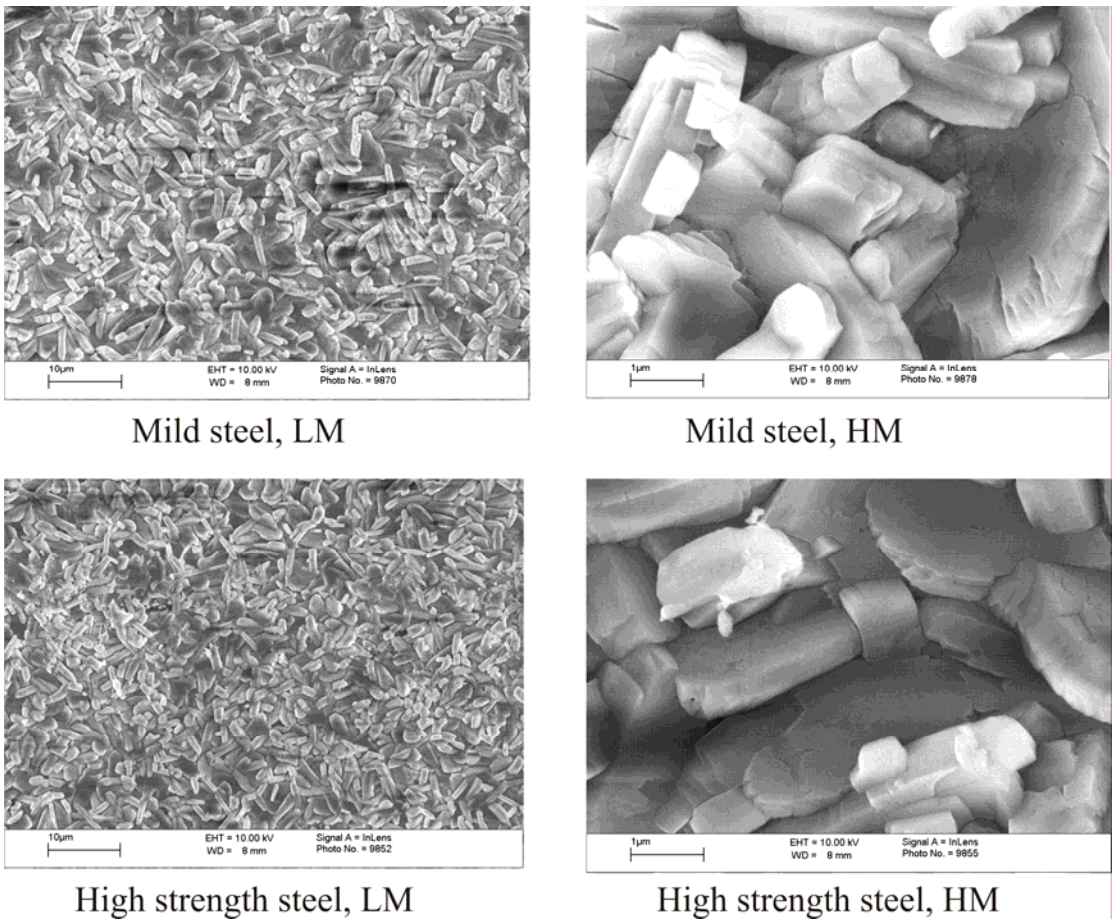

Figure 5 SEM images for A2 treatment of different steels (LM low magnification and HM high magnification).

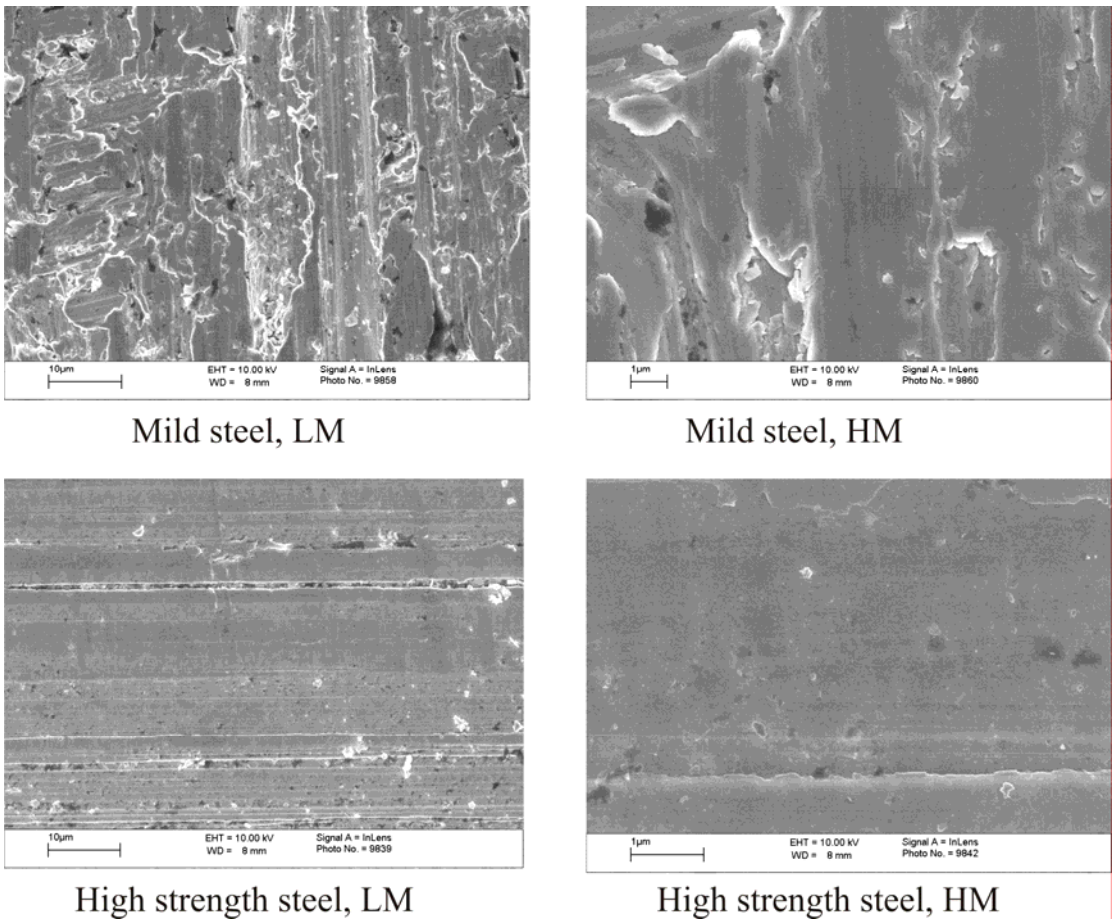

Figure 6 SEM images for P treatment of different steels (LM low magnification and HM high magnification).

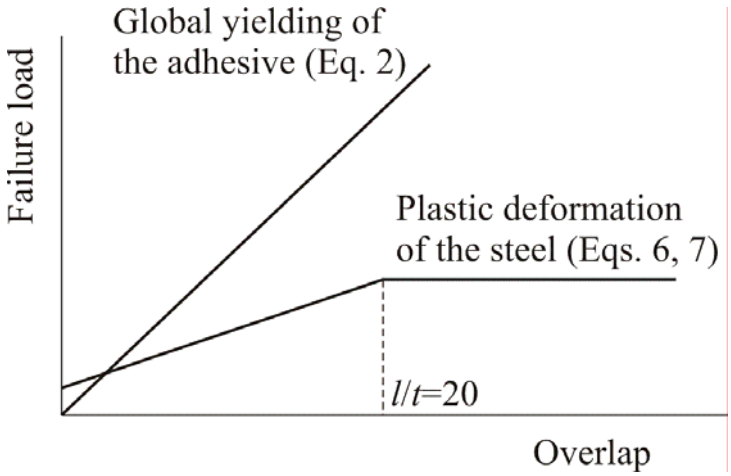

Figure 7 Methodology to predict the failure load of single lap joints as a function of overlap based either on the global yielding of the adhesive or on the plastic deformation of steel.

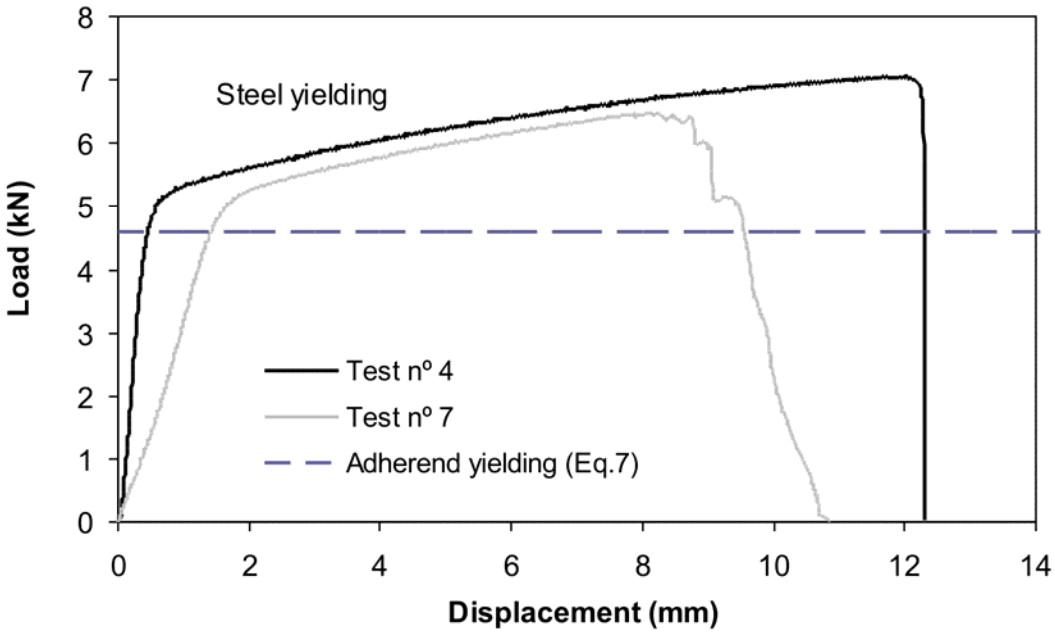

Figure 8 Load-displacement curves for tests nº 4 and 7 (see **Table 3**) and adherend yielding prediction using **Equation 7**.

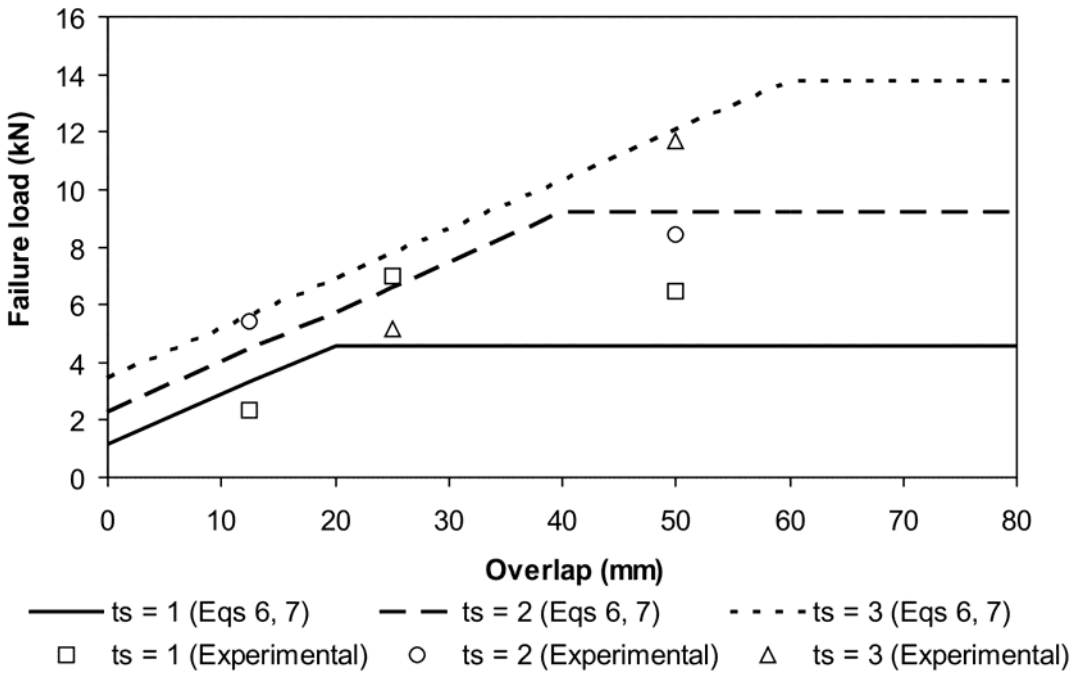

Figure 9 Experimental points corresponding to mild steel along with the three curves corresponding to the predictions for t_s =1, 2 and 3 mm using Equations 6 and 7 (adherend plastic yielding).

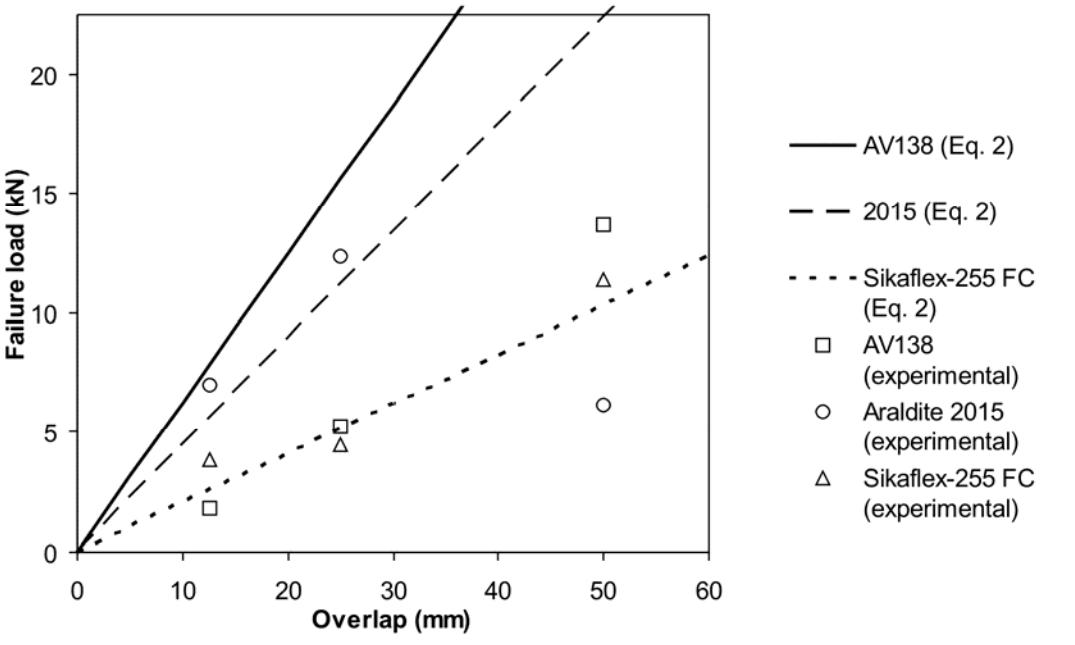

Figure 10 Experimental points corresponding to hard steel along with the three curves corresponding to the predictions for adhesives 2015, AV 138 and Sikaflex-255 FC using Equation 2 (adhesive global yielding).

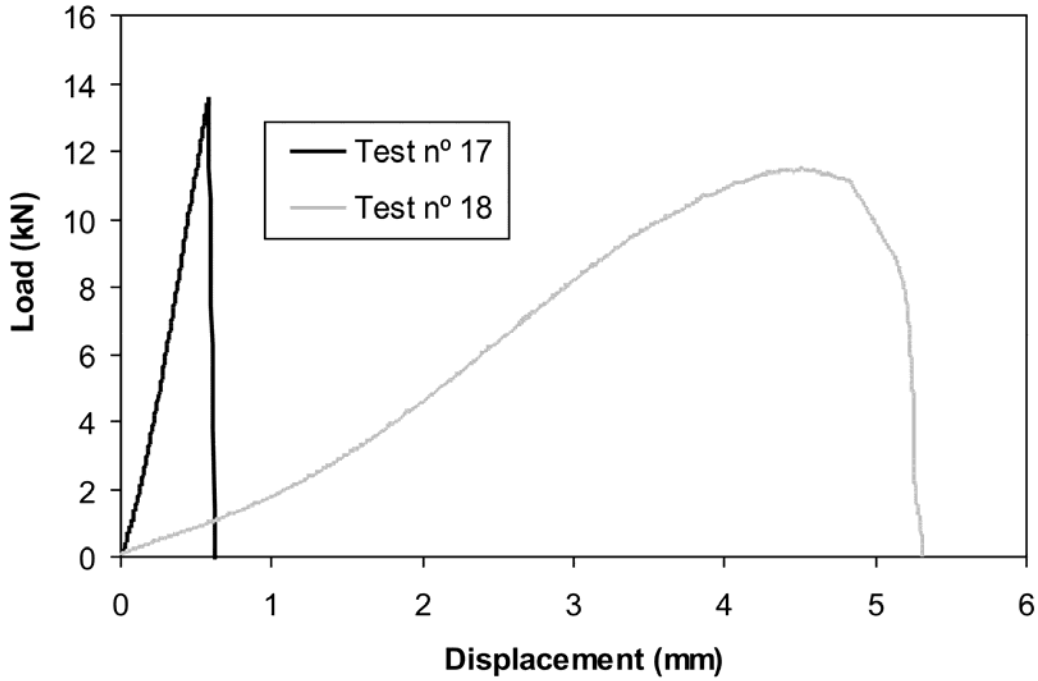

Figure 11 Load-displacement curves for test nº 17 and 18 (see **Table 3**)

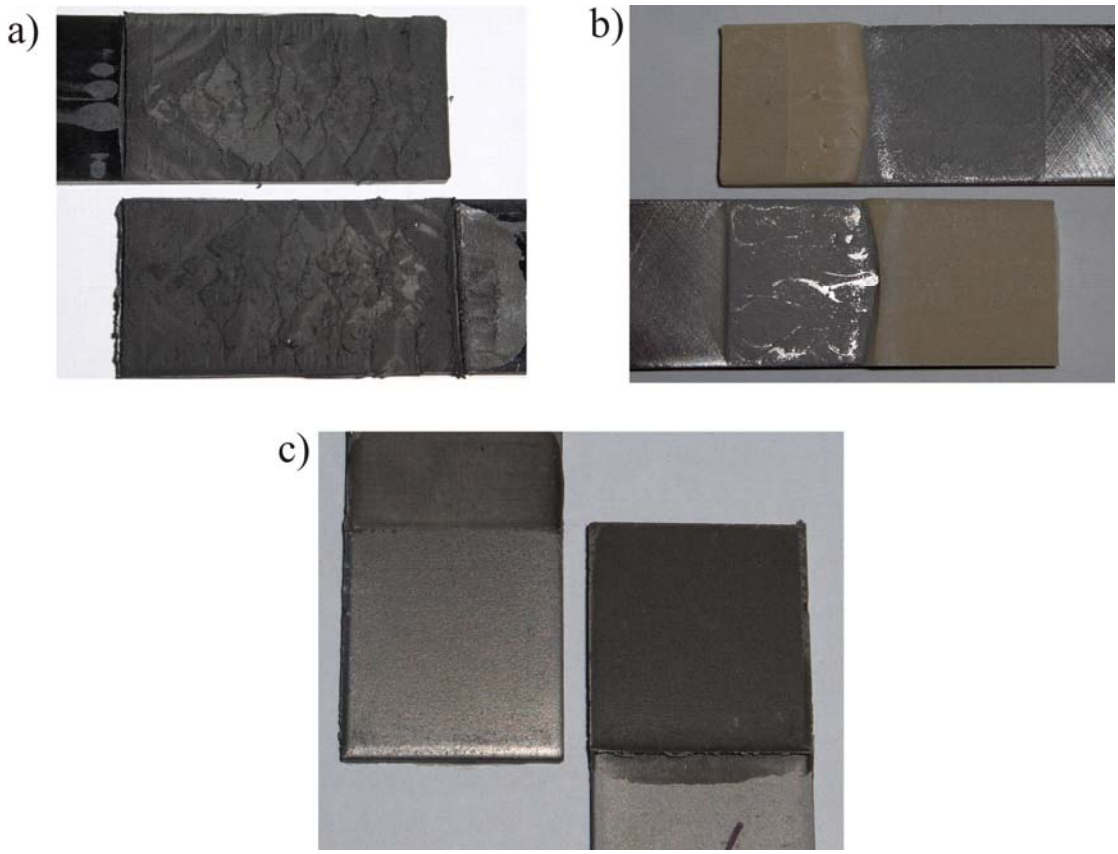

Figure 12 Failure surfaces; a) cohesive (test nº 18); b) cohesive close to the interface (test nº 8); c) adhesive (test nº 5).

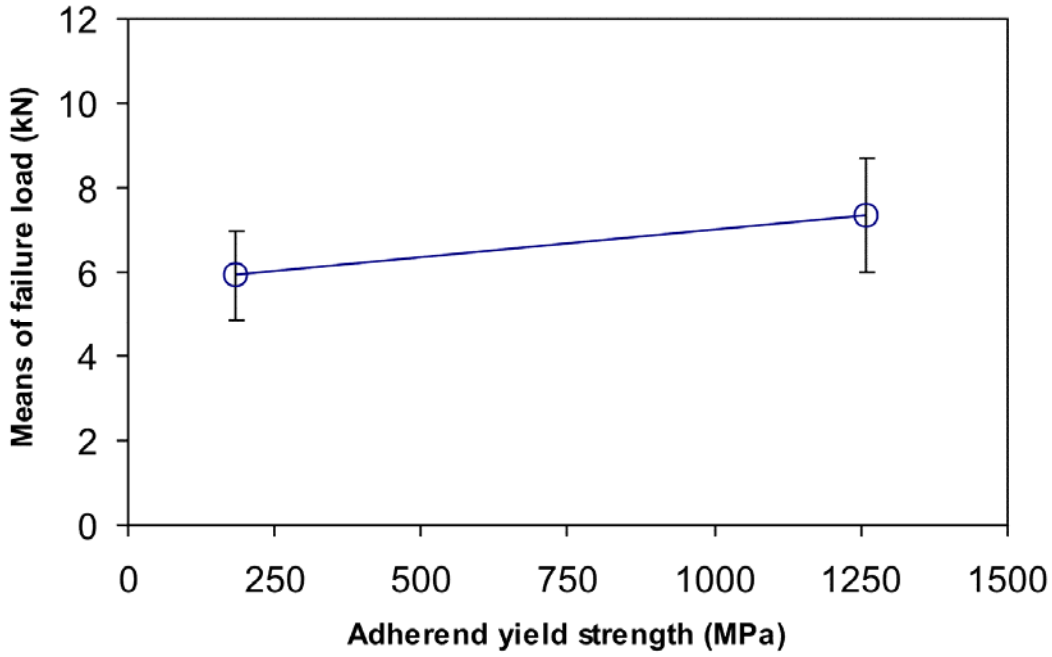

Figure 13 Average response graph with 95% confidence error bars for the main effect of adherend yield strength.

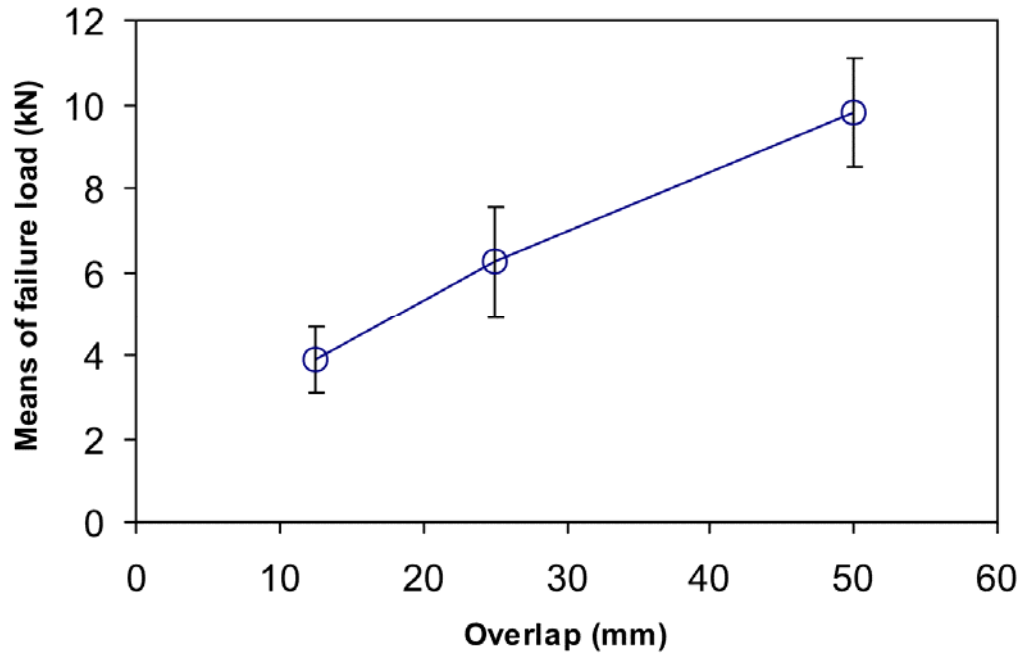

Figure 14 Average response graph with 95% confidence error bars for the main effect of the overlap.

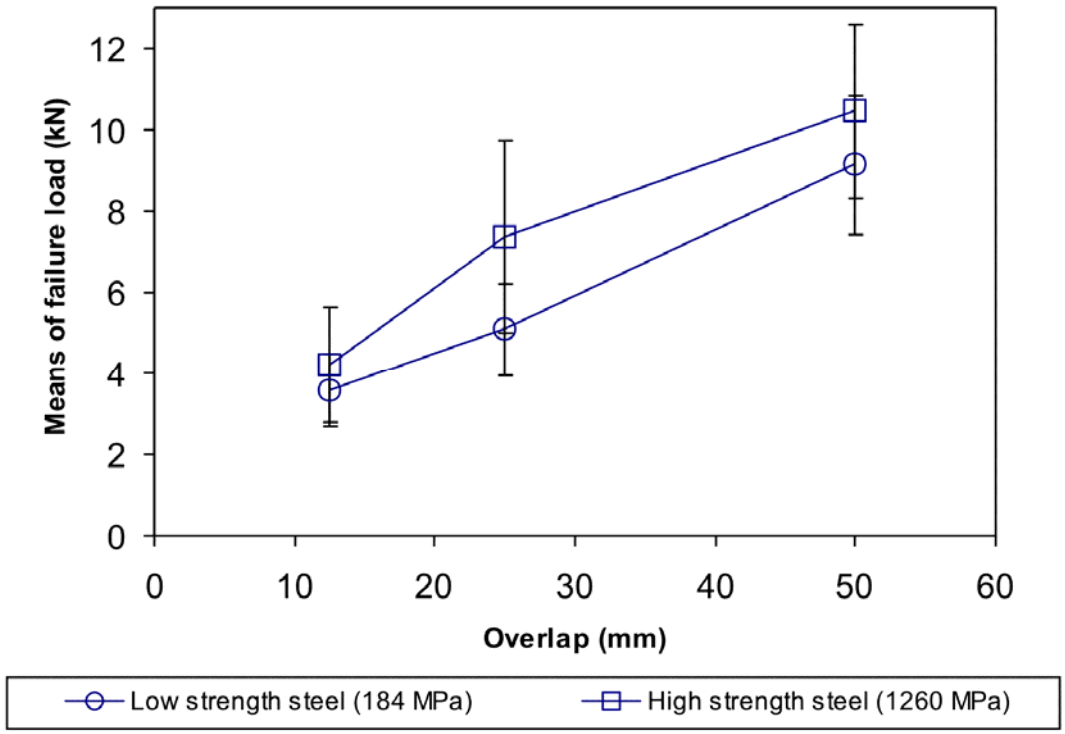

Figure 15 Average response graph with 95% confidence error bars for the main effect of the interaction adherend yield strength * overlap.

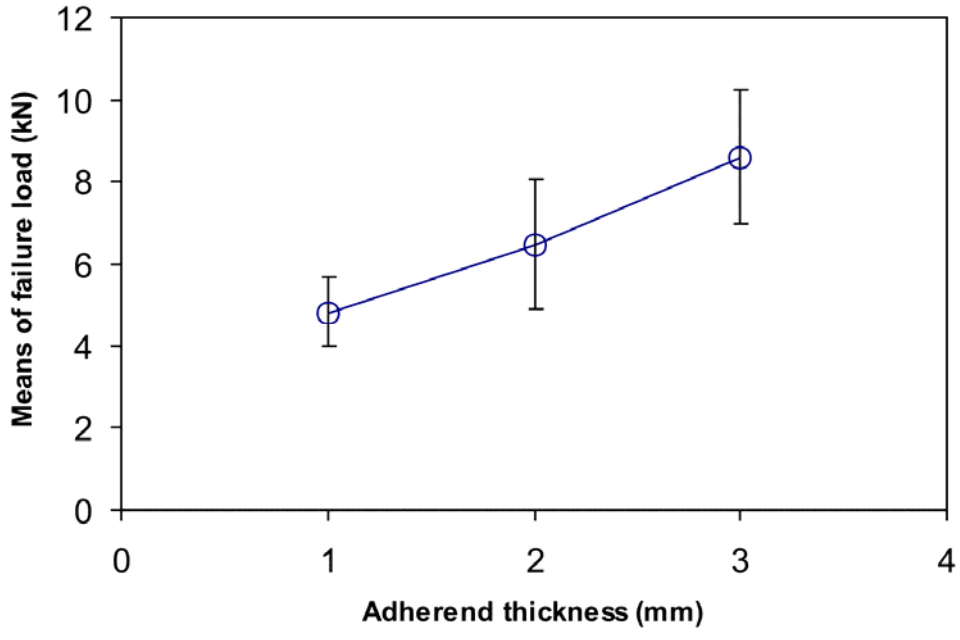

Figure 16 Average response graph with 95% confidence error bars for the main effect of the adherend thickness.

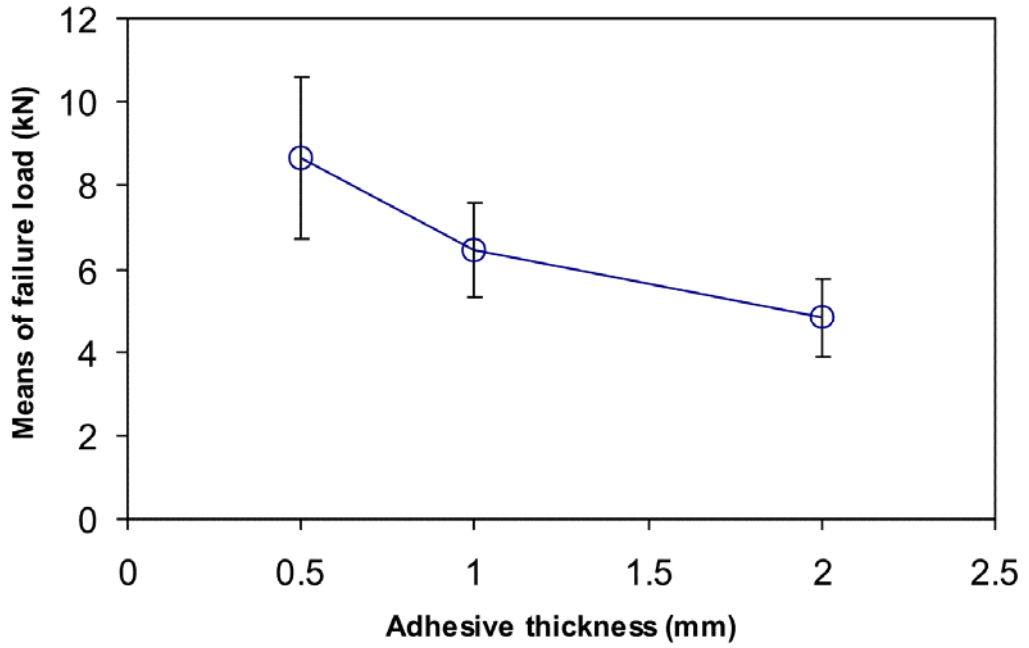

Figure 17 Average response graph with 95% confidence error bars for the main effect of the adhesive thickness.

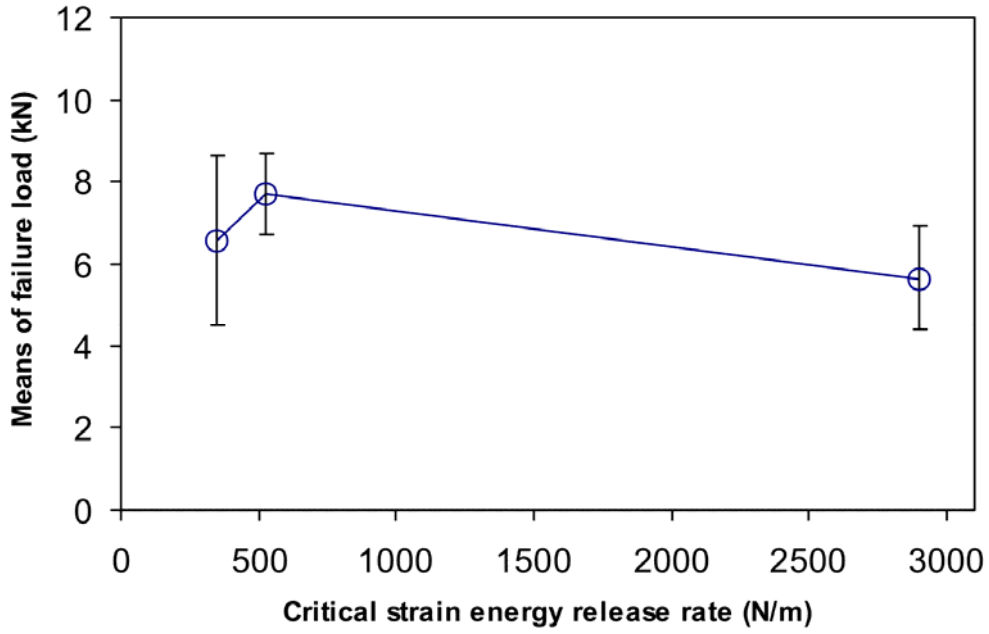

Figure 18 Average response graph with 95% confidence error bars for the main effect of the adhesive toughness.

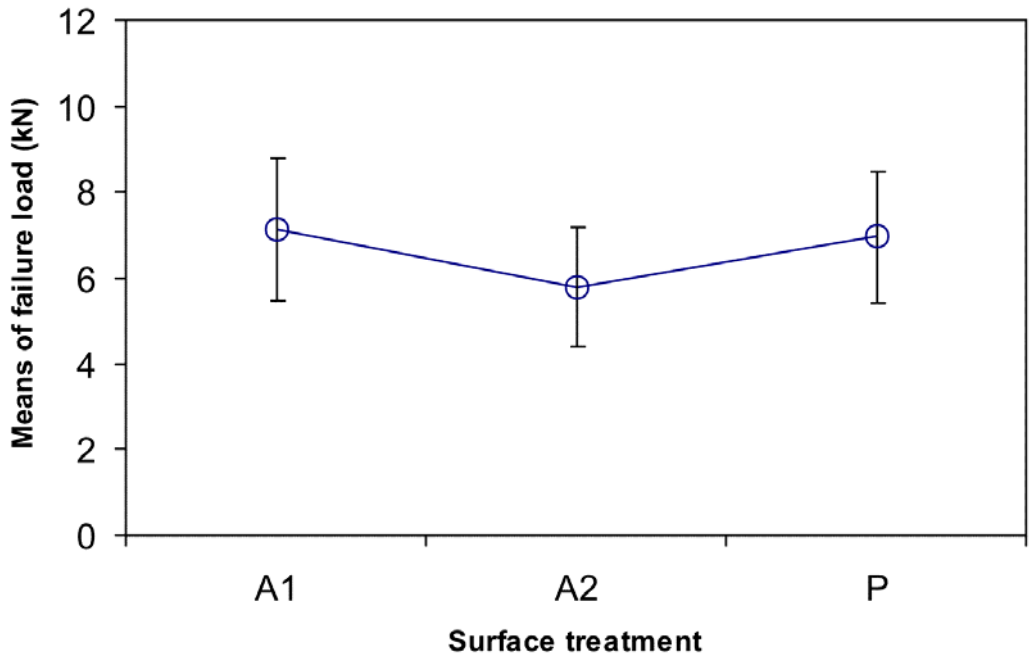

Figure 19 Average response graph with 95% confidence error bars for the main effect of the surface treatment.

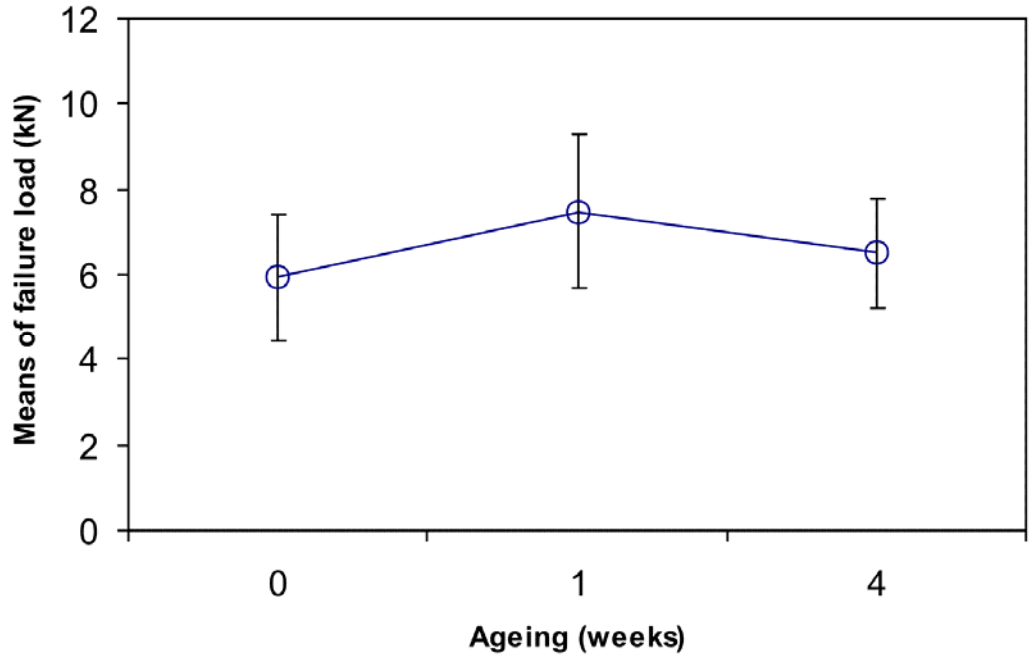

Figure 20 Average response graph with 95% confidence error bars for the main effect of the durability.

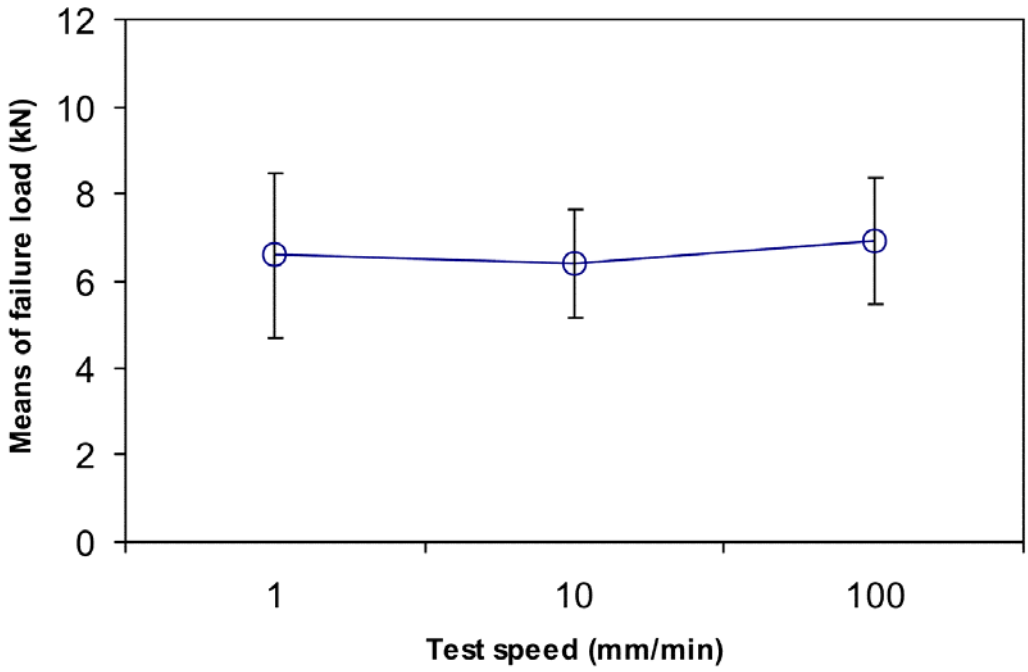

Figure 21 Average response graph with 95% confidence error bars for the main effect of the test speed.